Available online at www.sciencedirect.com
SCIENCE DIRECT®
PERGAMON
International Journal of Heat and Mass Transfer 46 (2003) 3313–3322
International Journal of HEAT and MASS TRANSFER
www.elsevier.com/locate/ijhmt

A numerical model for segmented flow in a microreactor

N. Harries [a], J.R. Burns [b], D.A. Barrow [a,*], C. Ramshaw [b]

[a] *Laboratory for Applied Microsystems, Cardiff School of Engineering, Cardiff University, Queen's Buildings, P.O. Box 689, Cardiff CF2 3TF, UK*

[b] *Department of Chemical & Process Engineering, University of Newcastle, Newcastle upon Tyne NE1 7RU, UK*

Received 6 August 2002

Abstract

A numerical model for segmented flow in a microreactor has been developed. The model is based on computational fluid dynamics (CFD) which means that the flow field and mass transfer are described by a set of partial differential equations. A general purpose CFD code was extended in order to predict the internal flow patterns of fluid segments and the transfer of dissolved chemical species within segments and across fluid segment interfaces. The model has been validated by comparing predicted data with experimental microreactor titrations.

Keywords: Numerical model; Segmented flow; Microreactor; Computational fluid dynamics

1. Introduction

Many industrially important chemical processes involve multiphase flow where reactions are led by diffusion across the contacting fluid phases, for example, gas–liquid hydrogenation and immiscible liquid–liquid nitration [1]. Developments in fabrication methods for microfluidic devices are increasingly providing this area of chemistry with opportunities to take advantage of the benefits of downscaling [2]. Microreactors based on multiphase flow have emerged in the last few years. These are mainly gas–liquid systems employing bubbly or segmented flow, an example of which is described by Hessel et al. [3]. More recently, attention has been paid to immiscible liquid–liquid systems at microscale with a focus on intensification of reactions in these systems by segmentation of the fluids. Liquid–liquid contacting devices most commonly use diffusion between parallel streams of the two phases as described by Harper [4] and Harston et al. [5]. The use of segmented flow to enhance diffusion in a liquid–liquid microreactor is demonstrated by Burns and Ramshaw [1,6]. Vortex flow patterns generated by the shearing motion within fluid segments enhances mixing within segments and improves mass transfer across the interface.

Efficiency of segmented flow systems in terms of reaction time is influenced by a number of factors including flow velocity, slug length, channel size, and liquid viscosity ratio. Slug length depends upon flow velocity, channel geometry, liquid viscosity and surface properties [1]. The complex relationship between design parameters for the segmented flow microreactor means that optimisation of the system can involve extensive experimental work. A predictive model for the flow field and mass transfer in a liquid–liquid segmented flow system would provide a design tool offering a faster and cheaper design process. Such a model would predict the mass transfer performance for a given segmented flow system. The model could be used to produce design guidelines, indicating the significance of individual design parameters on system efficiency, for microreactors with segmented flow.

Computational fluid dynamics (CFD) can provide detailed flow field information for fluid systems [7]. The method employed by CFD is to describe the flow with the governing conservation equations, which always include equations for the conservation of momentum

* Corresponding author. Tel.: +44-29-2087-5921; fax: +44-29-2087-4716.
E-mail address: barrow@cf.ac.uk (D.A. Barrow).

0017-9310/03/$ - see front matter
doi:10.1016/S0017-9310(03)00120-0

Nomenclature

s	seconds
t	time
u	momentum in the x-coordinate direction
u	velocity field
v	momentum in the y-coordinate direction
w	momentum in the z-coordinate direction

Greek symbols

α_1	total mass of acid in water
α_2	total mass of acid in kerosene
μ	laminar viscosity
ρ	fluid density

Other symbols

L	slug length (μm)
W	channel width (μm)
S_y	source term for y-momentum equation

(Navier–Stokes equations) and mass and may also include equations for the conservation of energy, concentration of chemical species and other scalar variables depending on the flow under investigation. This set of partial differential equations provides continuous data for the flow domain, however, direct solution of this equation set is not possible. The flow domain is divided into a mesh of volumes and the partial differential equations are discretised over the computational mesh yielding a set of algebraic equations which are then solved by an iterative calculation procedure. Solution of the algebraic equation set provides velocity, pressure and scalar (such as, temperature and concentration of chemical species) data for each mesh volume in the fluid domain. This vast array of solution data is processed to provide graphical representations of the solution in the form of speed maps, velocity vectors, streamlines and scalar concentration maps [8].

Availability of fast processors, computer memory and advanced graphics capabilities at reasonable cost together with commercially available user friendly CFD codes has meant that most areas of fluid engineering now use CFD as a design or research tool [8]. A number of commercially available CFD codes exist which are appropriate for microfluidic applications. The majority of these are general purpose codes, such as CFX, property of AEA Technology plc. [9], and FLUENT, property of Fluent Inc. [10]. A small number of available codes are designed specifically for microfluidic applications with preset options for microfluidic geometries and flow regimes, for example, CoventorWare, property of Coventor, Inc. [11]. Most commercial CFD codes are user friendly but vary in the add-on models they provide which may include models for particle tracking or chemical reaction. Codes also vary in the flexibility they offer for user development.

A numerical model for segmented flow in a microreactor was developed and validated in this study. Model development involved extending a CFD code to predict the flow field and mass transfer for immiscible liquid–liquid segmented flow. The numerical predictions for this study were performed with the CFD code CFX, which is a general purpose commercial code offering a range of add-on models appropriate for microfluidic applications and sufficient access to the source code to enable user software developments.

Microreactor experiments carried out at Newcastle University provided data which was used to validate the model [1]. Titration reactions were carried out to demonstrate the mass transfer performance of segmented flow. Predicted data was compared with experimental titration times and with photographic images of segmented flow titration.

Development and validation of the model are described in this paper.

2. Segmented flow

Segmented flow is comprised of alternating aqueous and organic segments (see Fig. 1). The aqueous phases do not mix but transfer of momentum (effects of vis-

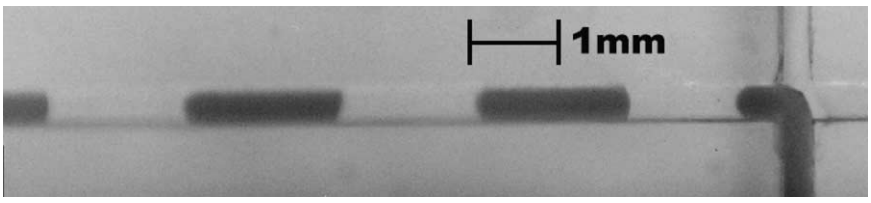

Fig. 1. Photographic image of liquid/liquid segmented flow in a microchannel (kerosene/water).

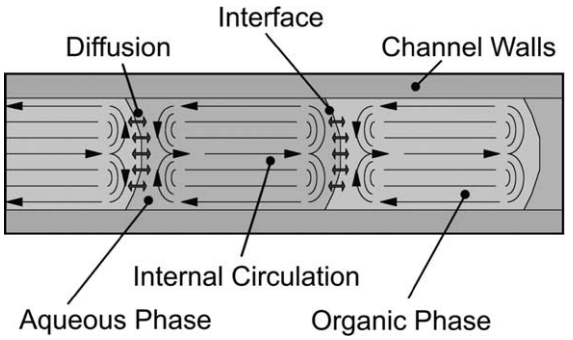

Fig. 2. Diagram illustrating the internal vortex flow patterns within fluid segments (flow direction is left to right).

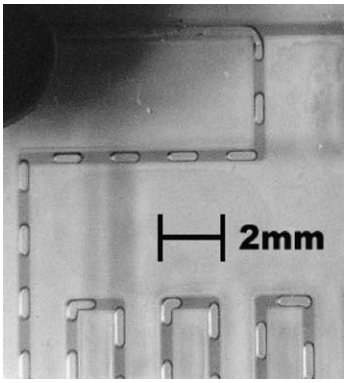

Fig. 3. Photographic image of fluid segments generated with a "T" piece.

cosity) and mass (dissolved chemicals) occurs across the fluid interface. As the fluid segments move along the channel internal vortex flow patterns are generated (see Fig. 2). These circulation patterns are a result of shearing motion within the low Reynolds number flow combined with fluidic interfaces. This fluid motion enhances mixing within the fluid segments and also improves the rate of diffusion of solute across the liquid/liquid interface by the shearing disruption of concentration gradients within the segments.

The alternating segments of two liquid phases provide an environment for mass transfer and chemical reaction. Typically, in segmented flow microreactors, solute in one phase diffuses into the adjacent segments where it reacts with dissolved chemicals in that phase. This study is concerned with modelling titration reactions in segmented flow, where acetic acid dissolved in the organic phase (kerosene) partitions into the aqueous phase and neutralises the dissolved base (KOH/NaOH).

Segmented flow may be generated in microchannels by various methods [1]. Commonly, a "T" shaped intersection is employed where the two liquid phases meet head-on [6]. Segments are generated by each phase cutting the flow of the other as both phases vie to travel down the exit channel (see Fig. 3). The model developed in this study represents established segmented flow. Modelling the generation of segmented flow is not within the scope of this report.

Glass microchannels of square cross-section and 380 μm wide were employed for the experimental titrations and fluid segments were generated using a "T" piece [1].

3. Computational fluid dynamics model

Segmented flow was represented by two adjacent rectangular units in a microchannel with moving walls (see Fig. 4). The fluid segments under observation were held in the calculation domain while the moving walls created the flow field. The adjacent fluid segments were linked at both ends, much like a strip of paper wrapped around into a continuous loop. In this way, the fluid segments behaved as though they were in a channel of segmented flow experiencing the effects of momentum and mass transfer from both ends.

Two fluid phases were defined, identified by density and viscosity. Both phases were incompressible and Newtonian in their viscous behaviour.

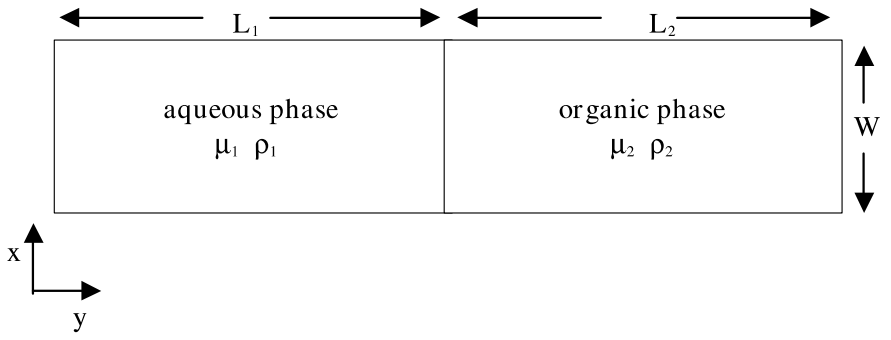

Fig. 4. Diagrammatic representation of modelled fluid segments.

A Cartesian coordinate system was employed with a no-slip condition applied to the channel walls. The axi-symmetric nature of the flow allowed a two-dimensional slice of the channel to be considered. The two-dimensional calculation permitted a high resolution computational mesh to be employed for the axial plane.

The interface between the fluid segments was assumed to be flat. An adjustment factor was applied to titration time to compensate for the reduced surface area resulting from the flat interface model. Alternative modelling options for the fluid interface are discussed in Section 6. The fluid interface was defined by setting zero axial velocity for the mesh cells which form the interface. This was achieved by setting the source terms for the v-momentum equation to zero (Eq. (1)—conservation equation for momentum in the y-coordinate direction [12]).

$$\frac{\delta(\rho v)}{\delta t} + \mathrm{div}(\rho \mathbf{u} v) = \mathrm{div}(\mu \,\mathrm{grad}\, v) - \frac{\delta \rho}{\delta y} + S_y \tag{1}$$

Diffusion of momentum and mass remained active across these cells. For momentum this is a condition of equal stress across the interface (Eq. (2)):

$$\mu_1 \delta u/\delta x = \mu_2 \delta u/\delta x \tag{2}$$

In addition to the boundary conditions at the interface between the fluid segments in the calculation domain, diffusion of mass and momentum were defined at the segment ends which formed connections with segments outside the calculation domain. Wall velocities were graduated to zero at the segment interfaces in order to maintain continuity of velocity in mesh cells near the boundaries. This approximate model for the fluid segment interface required a relaxation of viscosity ratio of the aqueous and organic phases in order to reach a converged solution with practicable computation times. A viscosity ratio of 1:1 was employed for the validation exercise. The calculated flow field is presented as a speed map with overlaid velocity vectors in Fig. 5. The vector map shows the vortex flow patterns within the fluid segments. Also, the wall velocity distribution is shown by the speed map.

The acid/base reaction in Eq. (3) was implemented into the segmented flow model:

$$KOH + CH_3COOH = CH_3COO^-K^+ + H_2O \tag{3}$$

Acid was initialised in the organic segment to represent acetic acid in kerosene. Solute is identified in the CFD code by its diffusivity in each phase and is initialised by concentration. Assisted by the recirculating flow patterns within the fluid segments the acid diffuses into the aqueous segment. Concentration maps representing the distribution of acetic acid as it diffuses across the organic/aqueous are presented in Fig. 6.

The recirculating flow patterns act to refresh the acid concentration at the interface of the organic and inorganic segments. In the aqueous segment, the recirculating flow draws the acid away from the interface along the centre line. A true representation of movement of acetic acid from kerosene to water is partitioning 85:1 in favour of the water phase. The source terms of the scalar equation representing dissolved acid were calculated to represent the partitioning movement of acetic acid across the water/kerosene interface. Fig. 7 illustrates how the concentration of acid was recalculated for the mesh cells either side of the fluid interface. In the diagram α_1 and α_2 represent the total mass of acid in water and kerosene respectively. The numerical expressions below the mesh cell diagram indicate how α_1 and α_2 were redefined in the source terms of the scalar equation representing dissolved acid.

Partitioning now replaces diffusion of acid at both fluid interfaces. Concentration maps representing the distribution of acetic acid as it partitions across the organic/aqueous interface are represented in Fig. 8.

Solute was initialised in the aqueous segment to represent KOH in water. KOH remains in the aqueous phase. As acetic acid partitions into the aqueous phase the acid neutralises the base (Eq. (3)). Source terms for the scalar equations representing the dissolved acid and base were calculated to represent the titration reaction. Concentration maps representing diminishing base during titration are presented in Fig. 9.

Most of the problem definition for the segmented flow model was achieved by Fortran coded subroutines.

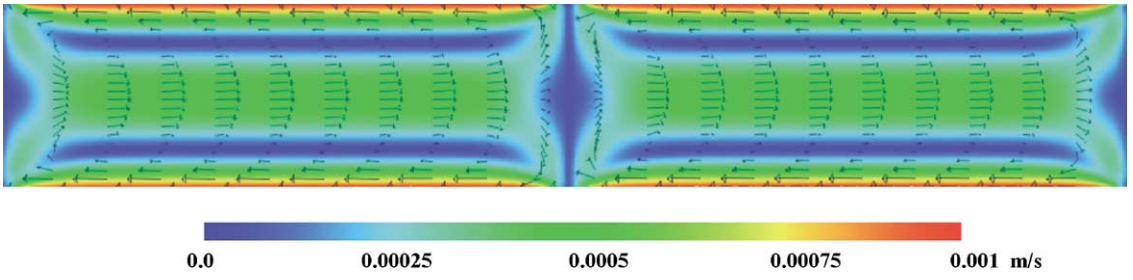

Fig. 5. Speed map and vectors representing calculated flow field.

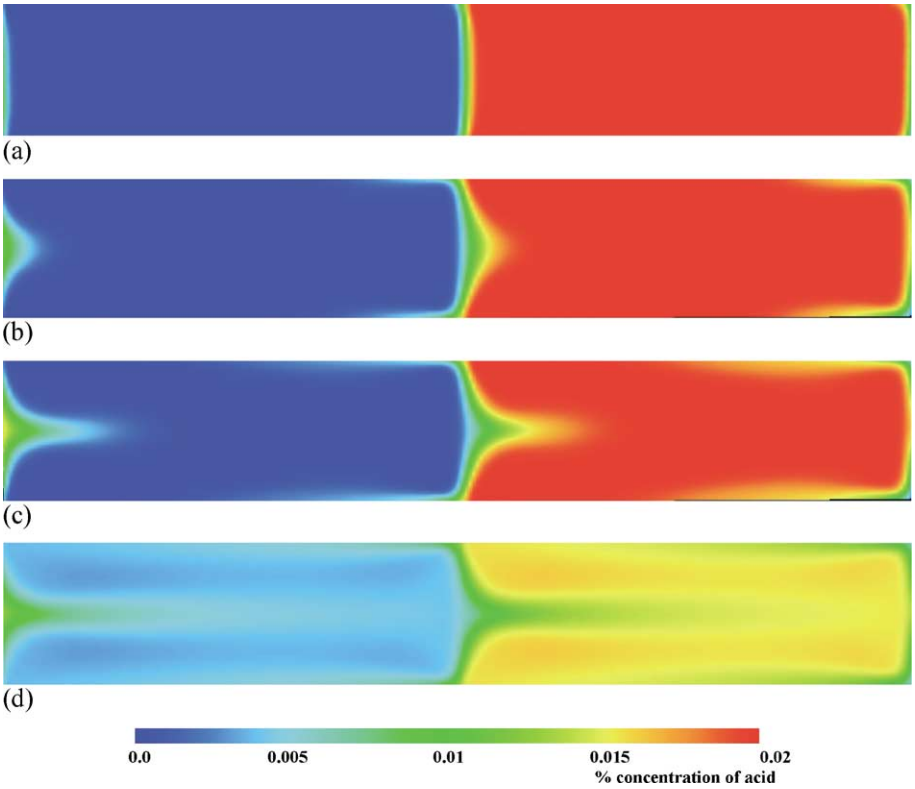

Fig. 6. Concentration maps representing the distribution of acetic acid as it diffuses from the organic to the aqueous phase (flow speed 0.1 mm/s). (a) $t = 0.1$ s, (b) $t = 0.5$ s, (c) $t = 1.0$ s, (d) $t = 6.0$ s.

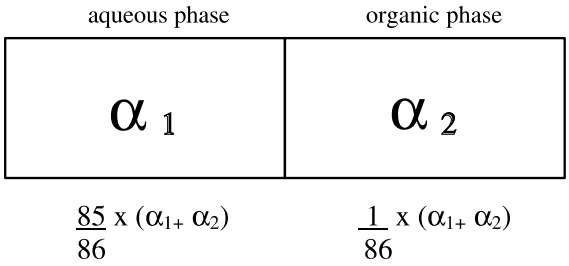

Fig. 7. Diagrammatic representation of mesh cell either side of fluid interface.

Two computers were used for running the CFD simulations in this study. A Sunblade100 Workstation (500 MHz processor, 256 MB memory and 15 GB internal disc) was used for course mesh simulations during code development. A Sun Enterprise 6500 (30×400 MHz processors with 6 GB memory) was used for the fine mesh simulations.

A computational mesh size of $0.001 \times$ slug length (1–2 μm mesh cells) achieved solutions with a high degree of mesh independency (50% change in mesh size producing less than 10% variation in solution data). During code development meshes of 10–20 μm, requiring short run times, were employed. Solutions for direct comparison with experimental titration employed a fine computational mesh (1–2 μm) to maximise accuracy. Fine mesh solutions require increased computer memory and storage, and have longer run times.

Converged flow fields were achieved with 100 time steps of 0.001 s with 50 iterations of velocity and mass equations at each time step. Up to this point in the solution the time steps have no physical meaning. The flow field is now established and the acid and alkali can now be initialised and time reset to zero. With the flow field frozen, that is zero iterations of the velocity and mass equations, the scalar variables were calculated with time steps of 0.001 s and 10 iterations of the scalar equations at each time step. Typically, computation time for a numerical solution to full titration is 30 h with a course mesh and 50 h with a fine mesh.

4. Model validation

Three sets of experimental titrations were modelled, each set representing a different base/acid concentration ratio. Table 1 indicates the base/acid ratios of the experimental titrations. A number of flow rates were

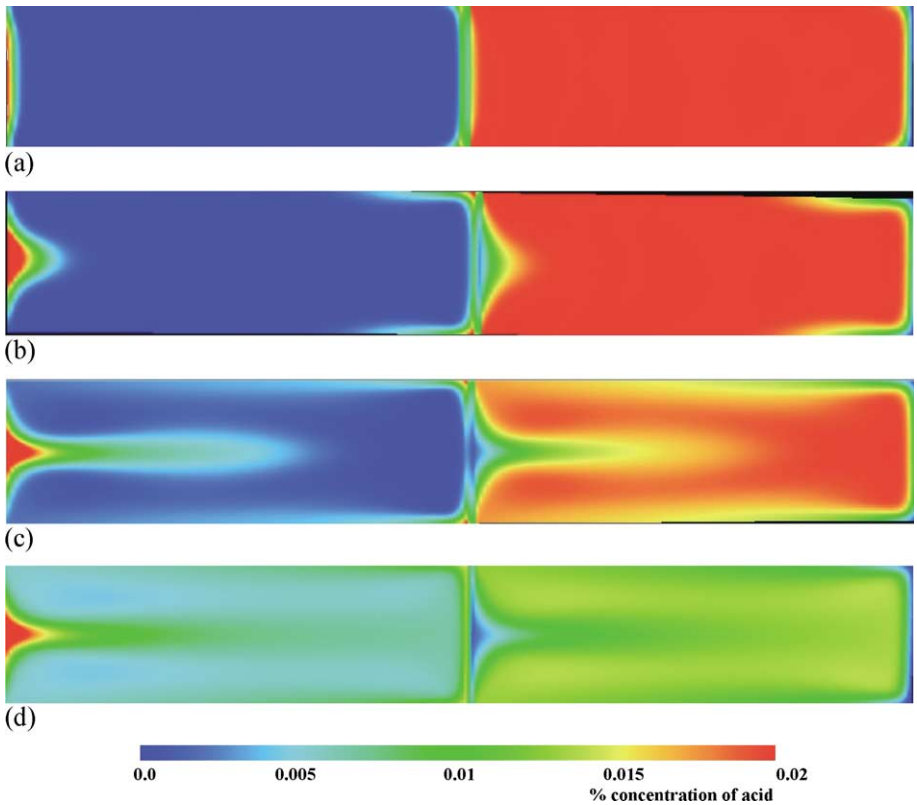

Fig. 8. Concentration maps representing the distribution of acetic acid as it partitions from the organic to the aqueous phase (flow speed 0.1 mm/s). (a) $t = 0.1$ s, (b) $t = 0.5$ s, (c) $t = 2.0$ s, (d) $t = 6.0$ s.

investigated within each set, these varied from 0.55 to 27.0 mm/s. Fluid segment length varied with flow rate with smaller segments being generated at higher speeds. Segment lengths were between 1 and 3.8 mm. At different acid/base concentrations the same flow rates did not produce the same segment length. This can be explained by the dependence of segment length on fluid properties. In order to compare experimental titration times with predicted values the concentration of base was averaged for the aqueous segment and the endpoint of titration was taken when 95% of the base had been neutralised.

5. Results

The predicted and experimental titration data were compared in the form of base concentration maps and titration times.

Figs. 10–12 graphically present the measured and predicted titration times for each base/acid ratio:

(i) titration time vs flow speed;
(ii) titration time vs segment length; and
(iii) measured vs predicted titration time.

The predicted titration times are similar to the experimental values for all three sets of data indicating that mass transfer has been predicted well by the model. The predicted titration times are all within 30% of the experimental times. The majority of predicted titration times (80%) are within 20% of the experimental values. The base concentration maps in Figs. 13 and 14 show similar distribution patterns. Fig. 13 is experimentally derived, whilst Fig. 14 is theoretically predicted. The similarity of the concentration maps qualitatively indicates that the general pattern of the flow is predicted well. Fig. 13 is a photographic image indicating the base distribution in an aqueous segment 4.0 s after slug formation at 2.8 mm/s. Fig. 14 is a concentration map representing the predicted base distribution in an aqueous segment 4.0 s after the start of titration at 2.8 mm/s. Comparison of the titration photograph in Fig. 13 with the predicted base map in Fig. 14 shows a similar distribution of base in the aqueous segment as it is neutralised during titration.

Titration time vs flow speed graphs show similar power law profiles for measured and predicted data (Figs. 10–12). This indicates a good prediction by the model of the influence of flow speed on titration time.

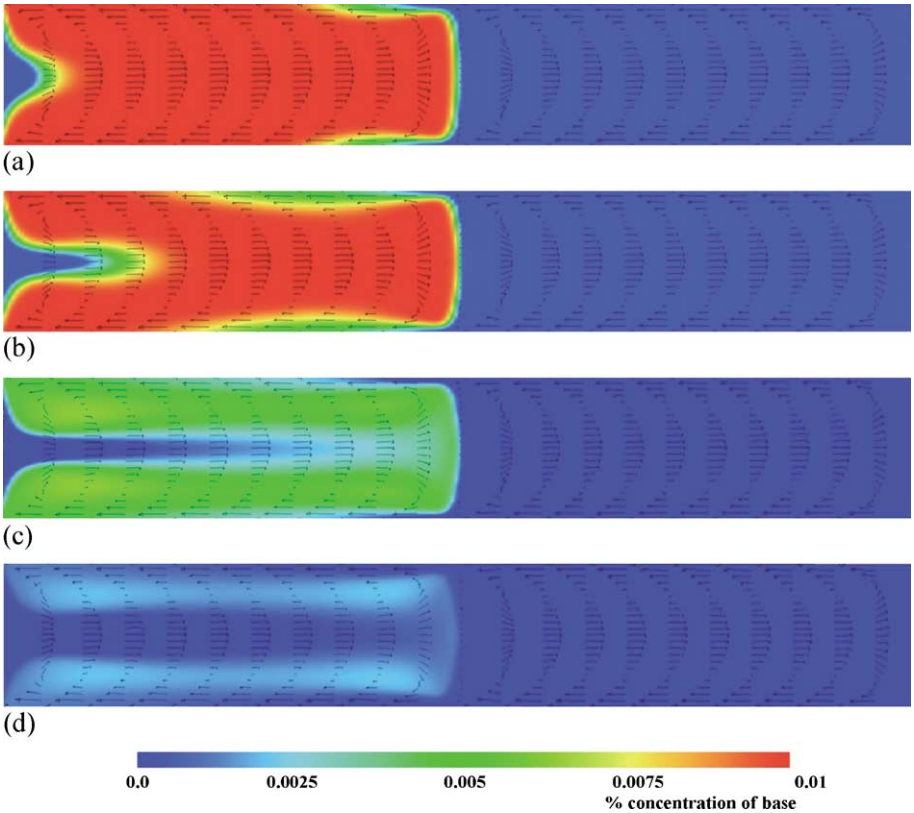

Fig. 9. Concentration maps representing the distribution of base during titration (flow speed 0.1 mm/s). (a) $t = 0.5$ s, (b) $t = 1.0$ s, (c) $t = 5.0$ s, (d) $t = 9.0$ s.

Table 1
Base/acid concentration ratios employed in the experimental titrations

Experiment	Base (moles/litre)	Acid (moles/litre)	Base/acid ratio
Titration (a)	0.25 NaOH	0.50 acetic	0.50
Titration (b)	0.25 KOH	0.68 acetic	0.37
Titration (c)	0.40 KOH	0.68 acetic	0.59

Similarly, titration time vs segment length correlation shows close power law profiles for the measured and predicted data (Figs. 10–12) indicating that the influence of segment length on titration time is well predicted.

The influence of base/acid concentration on titration time is accurately represented by the model. This can be seen from the close correlation between the simulated and experimental titration times for each of the base/acid concentration ratios.

Measured and predicted titration times show a high level of correlation (Figs. 10–12). R^2 values were 0.90, 0.96 and 0.92 for titrations (a), (b) and (c) respectively.

6. Discussion

Although the fluid segment interface was approximate in terms of both (i) the flat interface, (ii) wall velocities near the interface and (iii) relaxed viscosity ratio for the organic and aqueous phases, the overall performance of the model in predicting titration times and base distribution was good. A fine computational mesh (1–2 μm) was employed for the titration simulations. This brought the numerical solution data close to mesh independence. Finer computational meshes give greater solution accuracy but demand greater computational resources (CPU time, RAM and disk storage). A computer capable of running the model with a fine computational mesh would require at least a 400 MHz processor with 1 GB internal memory and 20 GB internal disc.

The model may be further refined by the implementation of a free surface model to provide a more accurate representation of the aqueous/organic segment interface. Representing the fluid segment interface in this way would allow the solution to exhibit finer details of the flow field, such as small vortices near the parabolic

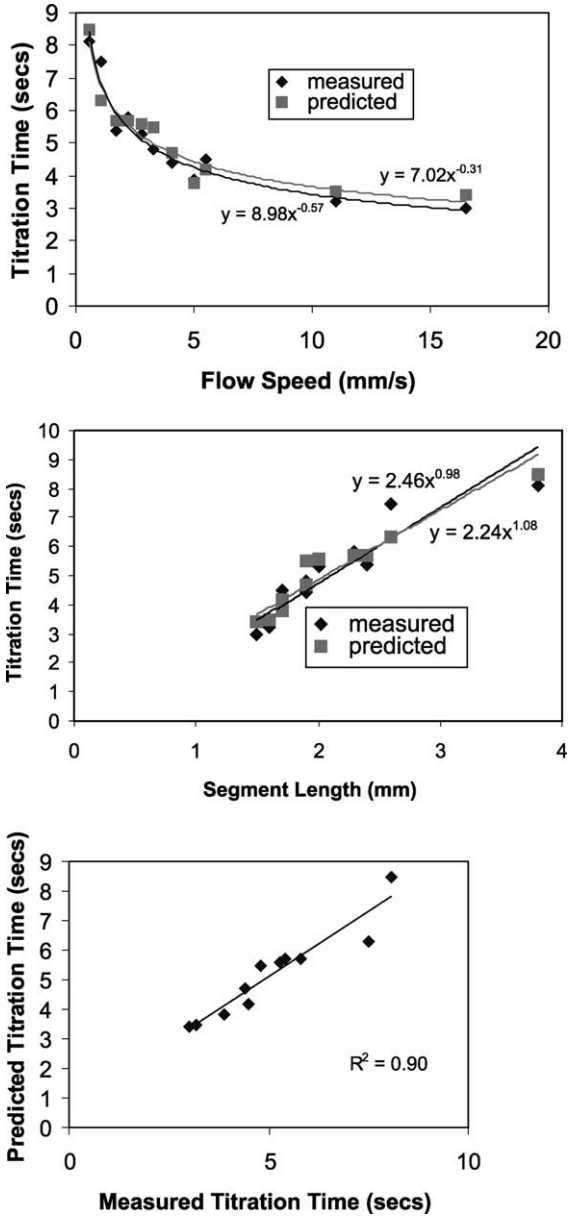

Fig. 10. Titration (a) data (base/acid mole ratio 0.5).

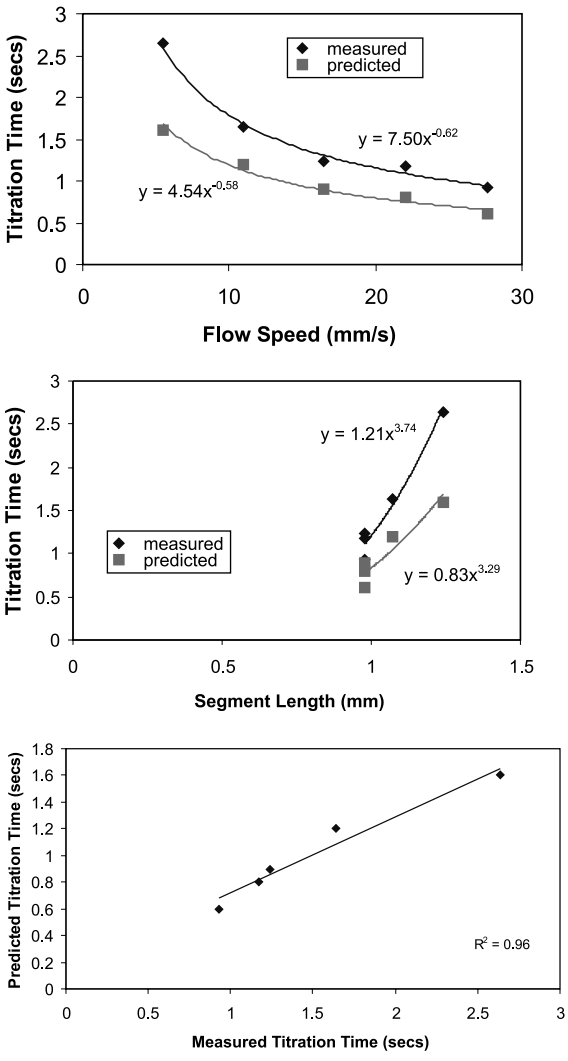

Fig. 11. Titration (b) data (base/acid mole ratio 0.37).

shaped interface. In turn, mass transfer would be more accurately represented. The continuum surface force (CSF) model developed by Brackbill et al. [13] and implemented into CFX by Burt et al. [14] would be appropriate for this purpose. Incorporating surface tension calculations into the segmented flow model would substantially increase the complexity of problem definition and the computational effort for solution. Following the implementation of a free surface model into the segmented flow model it would be appropriate to assess the gain in accuracy against the efforts to achieve a numerical solution. The model system employed in this report conveniently allowed the acquisition of laboratory experimental data to compare with theoretical predictions. Quantitative comparisons of experimental and predicted base concentration distribution are a subject for future research which would support the qualitative comparisons demonstrated in this study.

7. Conclusion

The validation results indicate that the model accurately predicts the flow field and mass transfer for the segmented flow system. This provides confidence in the model as a design tool for segmented flow in microreactors. However, numerical improvements to the nu-

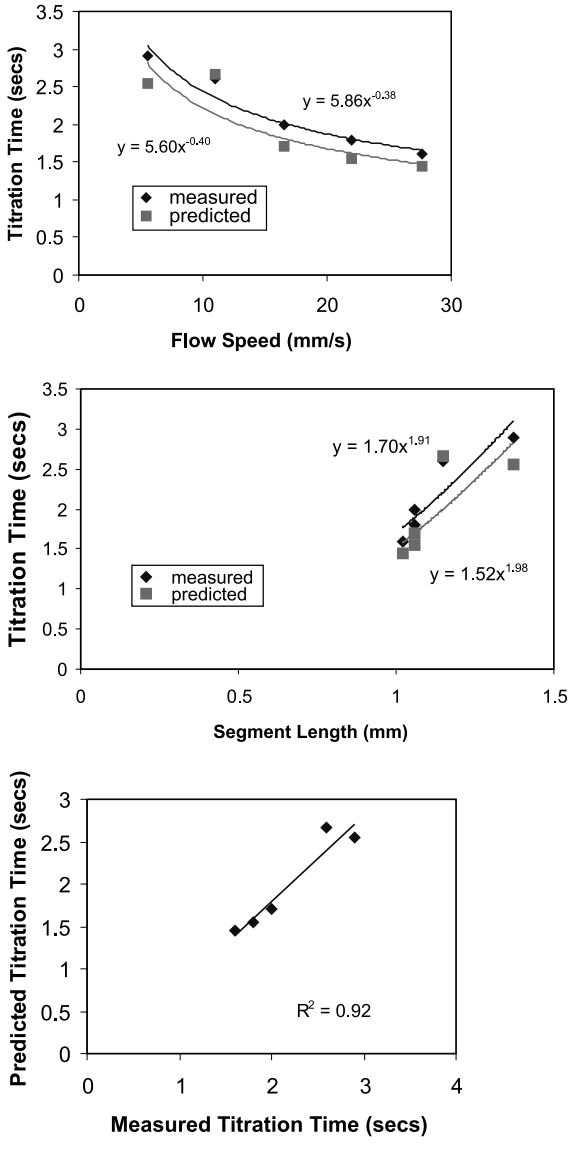

Fig. 12. Titration (c) data (base/acid mole ratio 0.59).

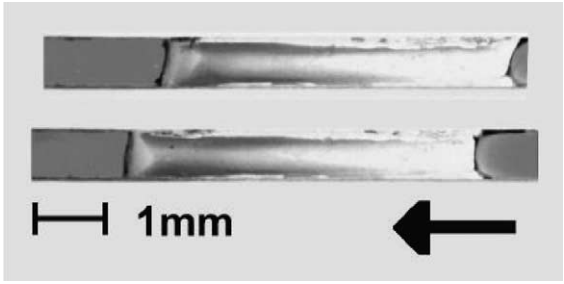

Fig. 13. Photographic image indicating base distribution during titration 4.0 s after slug formation (flow speed 2.8 mm/s).

merical model may be achieved by incorporating a free surface interface between contiguous segments and viscosity differentials. Performance of segmented flow may be assessed by using the model to predict mixing timescales for diffusion alone (static walls) and for segmented flow configuration at different speeds. The segmented flow model could be advantageously extended to calculate industrially important chemical reactions, such as the nitration of benzene or toluene. These complex chemical reactions would be implemented through the chemical kinetics routines already in place in CFX. Once again, the complexity of problem definition and the computational effort for solution would be substantially increased with the inclusion of chemical reaction calculations.

Acknowledgements

This research was supported through the UK Laboratory-on-a-Chip consortium comprising 17 UK based academic and industrial members and funded by the Engineering and Physical Science Research Council. Numerical predictions were performed with the CFD software CFX, property of AEA Technology plc. A Sun Enterprise 6500 computer was made available to this project by the Cardiff Centre for Computational Science and Engineering, Cardiff University.

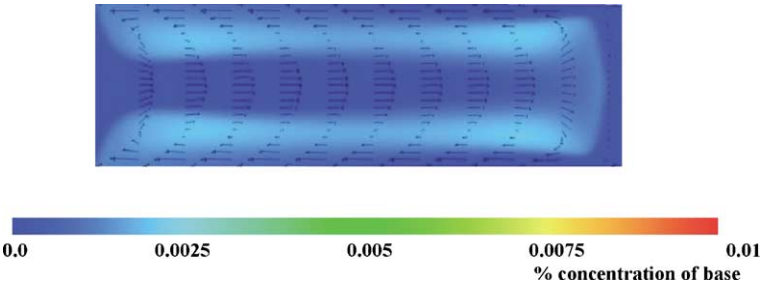

Fig. 14. Base concentration map of predicted titration after 4.0 s at 2.8 mm/s.

References

[1] J.R. Burns, C. Ramshaw, The intensification of rapid reactions in multiphase systems using slug flow in capillaries, Lab Chip J. (1) (2001) 10–15.
[2] E. Oosterbroek, Modelling, design and realisation of microfluidic components, Ph.D. thesis, University of Twente, Enschede, The Netherlands, 1999. ISBN 90-36513464.
[3] V. Hessel, W. Ehrfeld, Th. Herweck, V. Havercamp, H. Lowe, J. Sechiewe, Ch. Wille, Gas/liquid microreactors, in: Hydrodynamics and Mass Transfer, Proceedings of the 4th International Conference on Microreaction Technology, 2000, pp. 174–186.
[4] M.J. Harper, Method and apparatus for diffusive transfer between immiscible liquids, International Patent WO 97/39814, 1997.
[5] P. Harston, J.R. Burns, C. Ramshaw, Reactions of aromatic compounds, International Patent WO 99/22858, 1999.
[6] J.R. Burns, C. Ramshaw, A microreactor for the nitration of benzene and toluene, in: Proceedings of the 4th International Conference on Microreaction Technology, 2000, pp. 133–140.
[7] S.V. Patankar, Numerical Heat Transfer and Fluid Flow, Taylor & Francis, 1980.
[8] J.D. Anderson, Computational Fluid Dynamics, McGraw-Hill, 1995.
[9] CFX Update, Computational Fluid Dynamics Software and Services. ISSN 0965-1608, no. 21, Winter 2001.
[10] FLUENT User's Guide, vol. 4, 1996, Release 4.4, Fluent Europe Ltd., Sheffield.
[11] MEMS and Microsystems Design, Designer Reference and Tutorials, Coventor, Inc., 2001.
[12] R.W. Johnson, The Handbook of Fluid Dynamics, CRC Press and Springer-Verlag, 1998.
[13] J.U. Brackbill, D.B. Kothe, C. Zemach, A continuum method for modelling surface tension, J. Comput. Phys. 100 (1992) 355.
[14] D.J. Burt, J.W.J. Ferguson, H. Pordal, Numerical computation of surface tension effects, Proc. ASME 3 (1996) 439.